Supporting Information

Atomic-Layer-Deposition Process Enabled Carrier Mobility Boosting in Field-Effect Transistors through a Nanoscale ZnO/IGO Heterojunction

Hyeon Joo Seul,[†] *Min Jae Kim,*[†] *Hyun Ji Yang,*[†] *Min Hoe Cho,*[†] *Min Hee Cho,*[‡] *Woo-Bin Song*[‡] *and Jae Kyeong Jeong**[,†]

[†]Department of Electronic Engineering, Hanyang University, Seoul 04763, South Korea

[‡] Semiconductor R&D Center, Samsung Electronics Co., 1, Samsungjeonja-ro, Hawseong-si, Gyeonggi-do, 18448, Korea

AUTHOR EMAIL ADDRESS: J. K. Jeong (jkjeong1@hanyang.ac.kr)

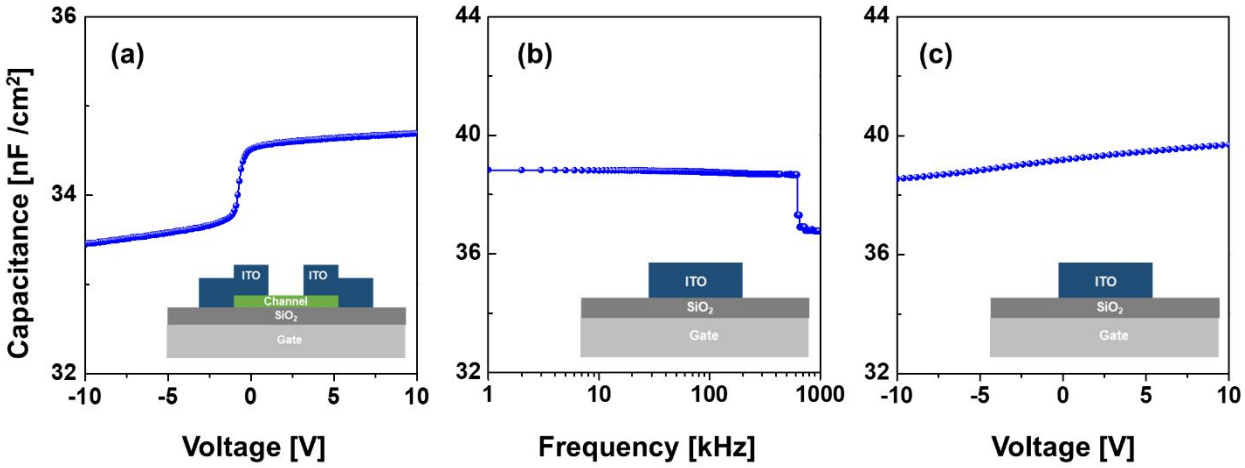

Figure S1. (a) Variations in areal capacitance as a function of gate voltage for the oxide FET device where the source and drain electrode are grounded. (b) Frequency and (c) voltage-dependent areal capacitances for the MIM capacitor with 100-nm-thick SiO_2 dielectric layer.

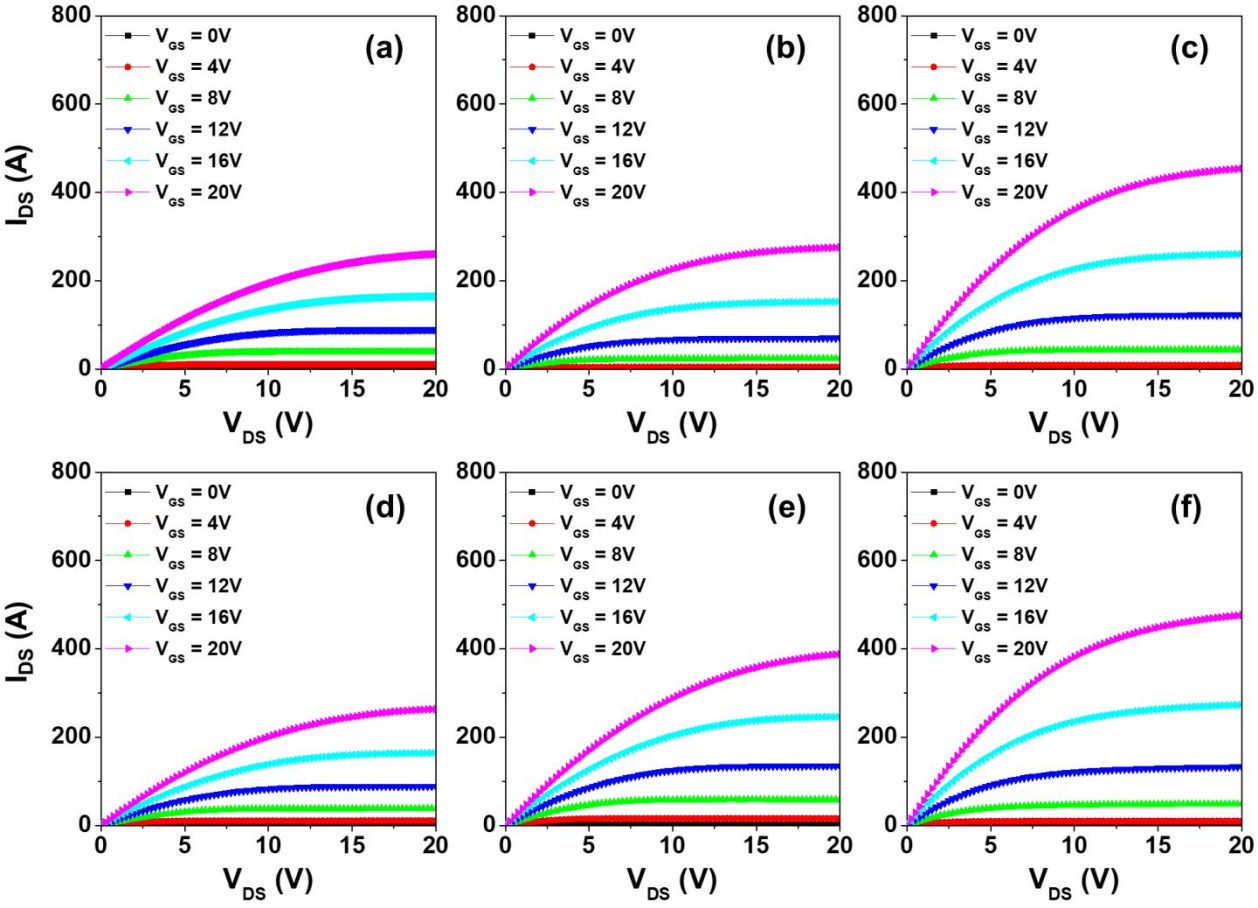

Figure S2. Corresponding output characteristics of FETs with (a) $In_{0.65}Ga_{0.35}O_{1.5}$, (b) $In_{0.75}Ga_{0.25}O_{1.5,}$ (c) $In_{0.83}Ga_{0.17}O_{1.5}$, (d) ZnO/$In_{0.65}Ga_{0.35}O_{1.5}$, (e) ZnO/$In_{0.75}Ga_{0.25}O_{1.5}$, and (f) ZnO/$In_{0.83}Ga_{0.17}O_{1.5}$.

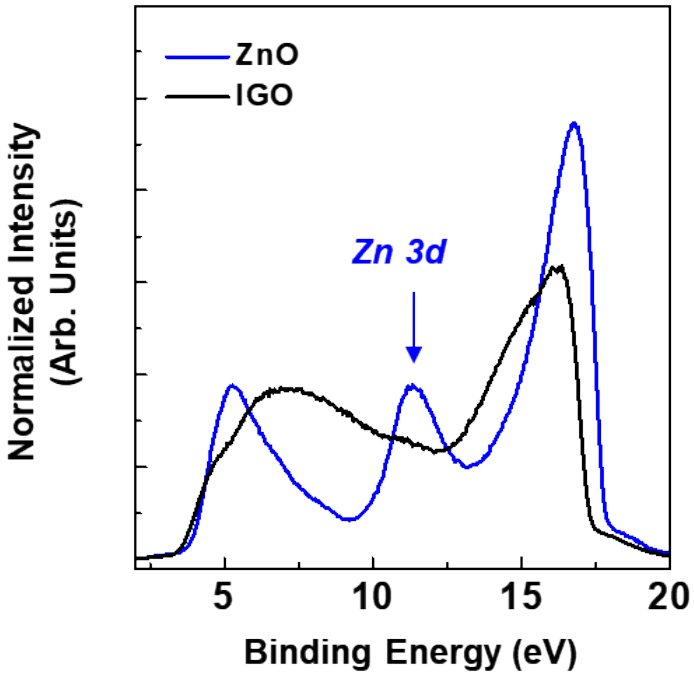

Figure S3. UPS spectra of ZnO and IGO thin film samples.

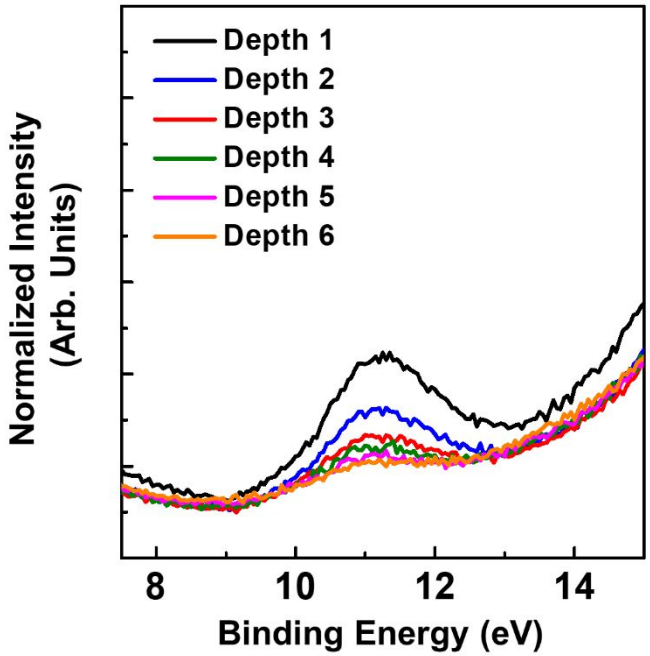

Figure S4. Zn 3d core-level emissions of ZnO/$In_{0.83}Ga_{0.17}O_{1.5}$ at different depths, based on UPS depth analysis.

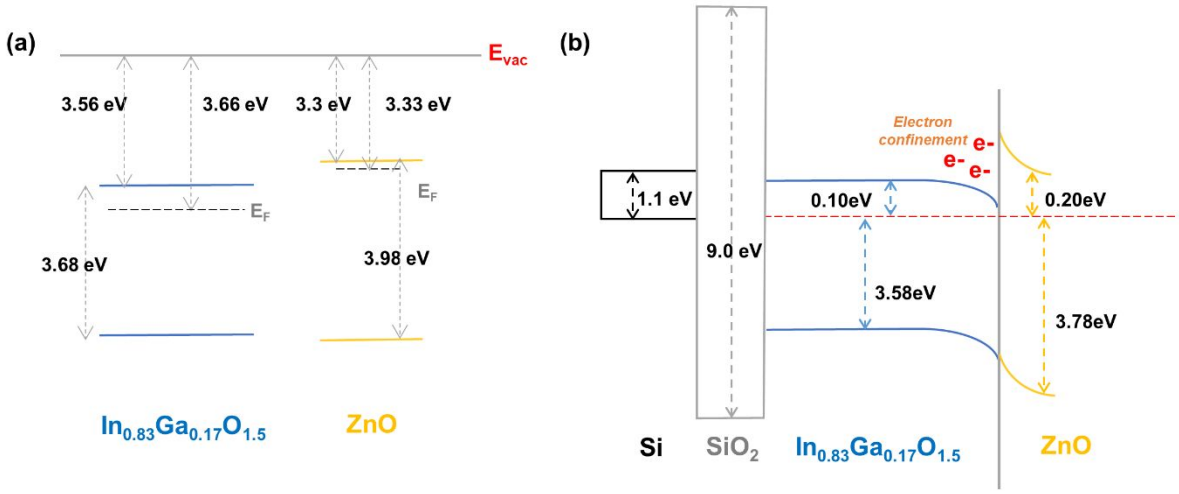

Figure S5. (a) Energy level of isolated $In_{0.83}Ga_{0.17}O_{1.5}$ and ZnO material. (b) Schematic energy band diagram of the ZnO/$In_{0.83}Ga_{0.17}O_{1.5}$ heterojunction. Using the $1/C^2$ vs V plot of MOS capacitor with the ZnO channel layer, we obtained the carrier concentration of ~ 5.0×10^{18} cm^{-3} and, thus, the E_F is located to be closed to its E_C, ($E_C - E_F \approx 0.03$ eV) as shown in Figure S5a. After contact between $In_{0.83}Ga_{0.17}O_{1.5}$ and ZnO, the free carriers in ZnO film fall into the $In_{0.83}Ga_{0.17}O_{1.5}$ region. The capping ZnO layer will be fully depleted due to the extreme thin nature of 3 nm. It can cause the separation between E_C and E_F at the back surface of ZnO by ~0.2 eV (Figure S5b), which was determined by UPS depth-profile analysis. This interpretation was also supported by TCAD simulation (Figure 10).

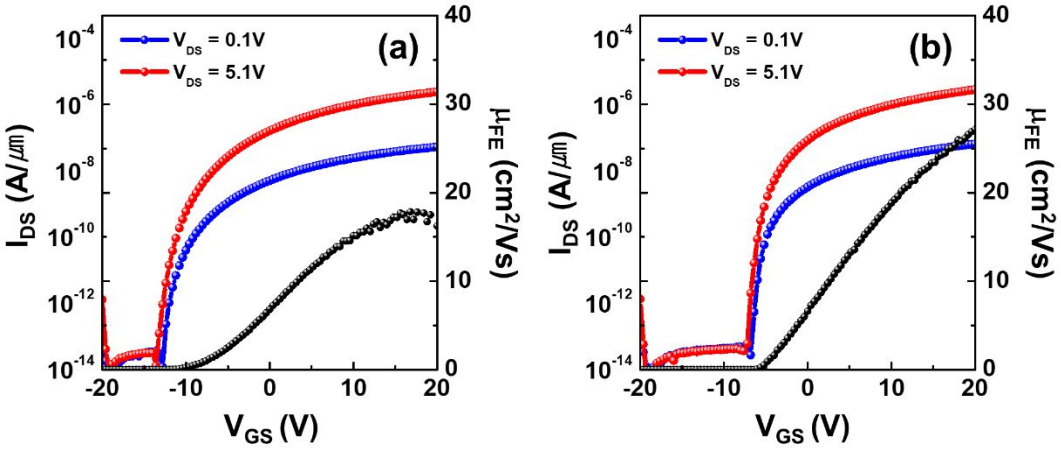

Sample	μ_{FE} (cm^2/V s)	SS (V/decade)	V_{TH} (V)	$I_{ON/OFF}$
In_2O_3	20.0 ± 2.1	0.92 ± 0.13	-12.0 ± 0.58	~ 10^8
ZnO/In_2O_3	27.1 ± 3.6	0.49 ± 0.21	-5.41 ± 0.36	~ 10^8

Figure S6. Transfer characteristics and electrical parameters of FETs with (a) In_2O_3 and (b) ZnO/In_2O_3 channel layers.

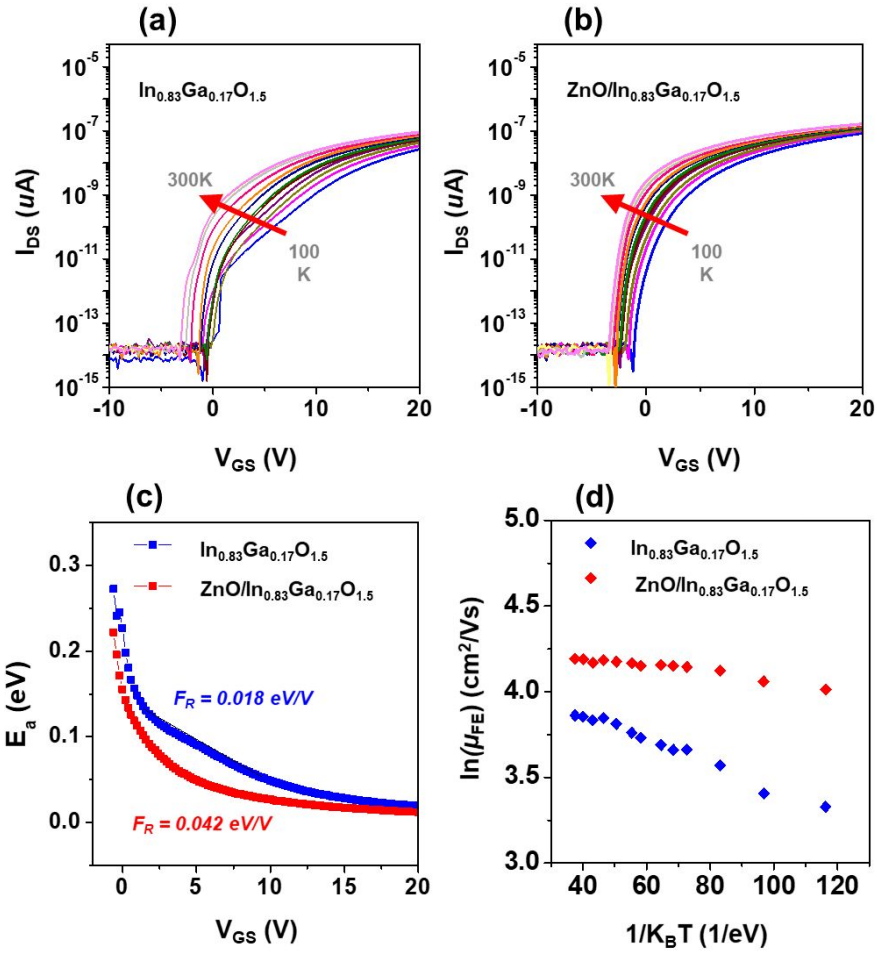

Figure S7. Temperature-dependent transfer characteristics for FETs with the (a) $In_{0.83}Ga_{0.17}O_{1.5}$ and (b) $ZnO/In_{0.83}Ga_{0.17}O_{1.5}$ channel layer in the range of 100-300 K. (c) Variation of activation energy (E_A) of the I_{DS} vs V_{GS}. (d) Arrhenius plot between 1/kT versus μ_{FE} value.

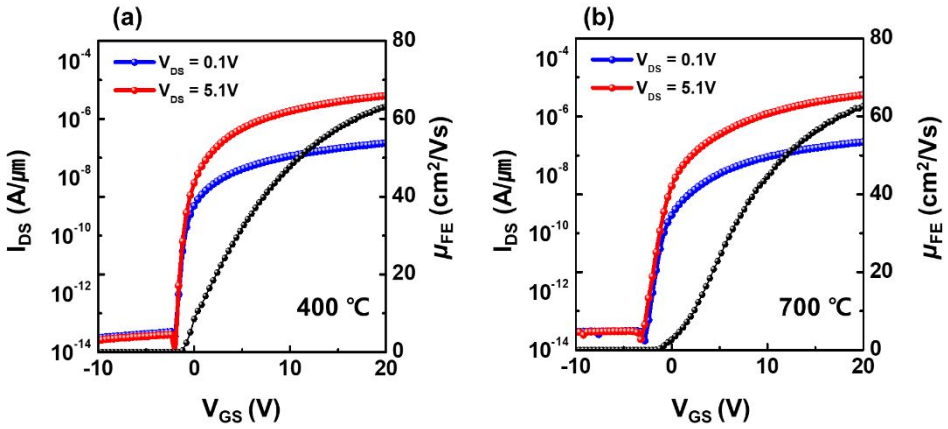

$ZnO/In_{0.83}Ga_{0.17}O_{1.5}$	μ_{FE} ($cm^2/(V\ s)$)	*SS* (V/decade)	V_{TH} (V)	$I_{ON/OFF}$
400 °C	63.2 ± 0.26	0.26 ± 0.03	-0.84 ± 0.85	$\sim 10^8$
700 °C	62.5 ± 0.42	0.52 ± 0.11	-0.83 ±0.88	$\sim 10^8$

Figure S8. Representative transfer characteristics of FETs with $ZnO/In_{0.83}Ga_{0.17}O_{1.5}$ heterojunction annealed at (a) 400 and (b) 700 °C. The important device parameters were summarized in Table (below).

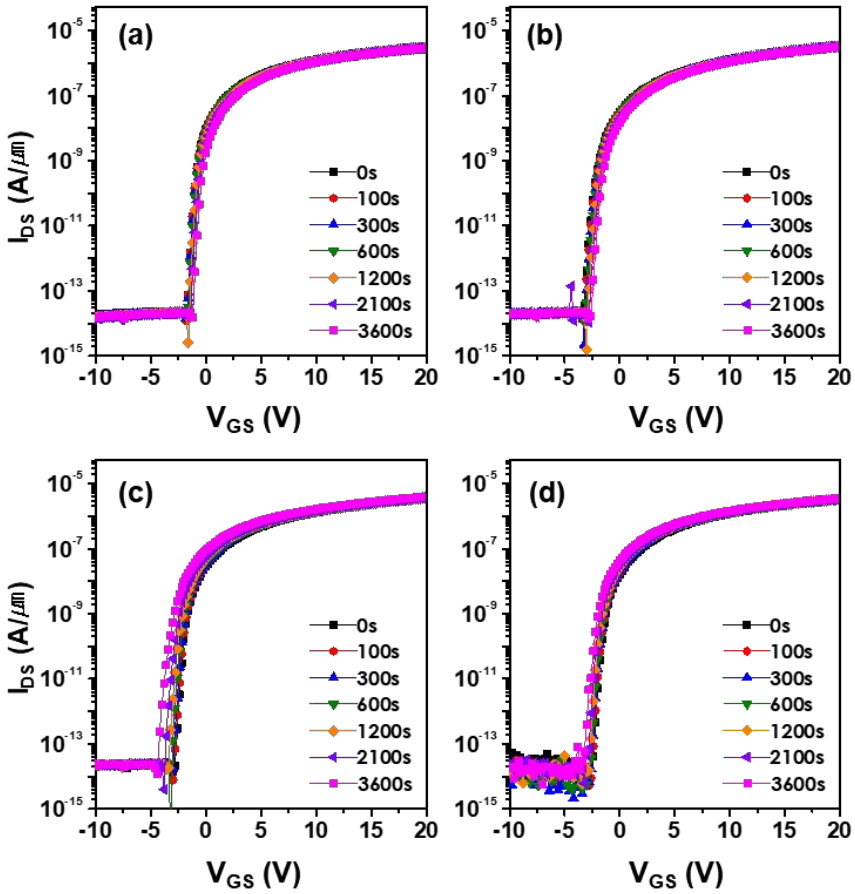

Figure S9. Variations in the time-dependent transfer characteristics for FETs with (a, b) $In_{0.65}Ga_{0.35}O_{1.5}$ and (c, d) $ZnO/In_{0.65}Ga_{0.35}O_{1.5}$ channel layers under (a, c) PBS and (b, d) NBS conditions. The stress conditions are as follows: PBS ($V_{GS} = V_{TH} + 20$ V) and NBS ($V_{GS} = V_{TH} - 20$ V).

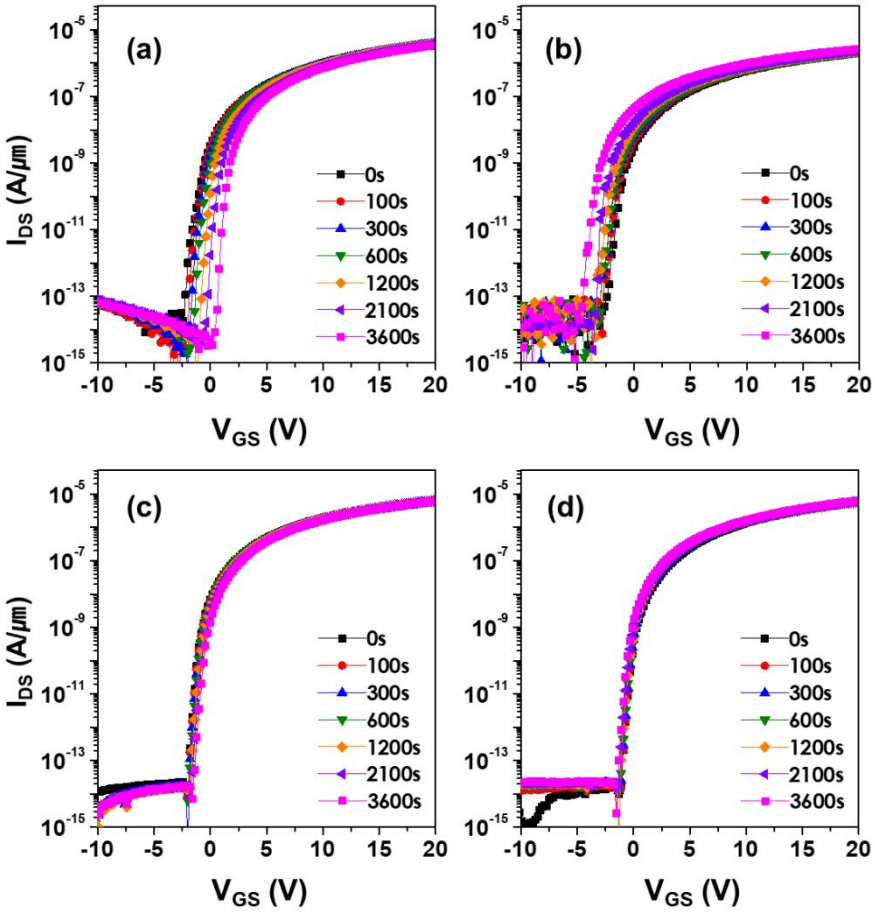

Figure S10. Variations in the time-dependent transfer characteristics for FETs with (a, b) $In_{0.83}Ga_{0.17}O_{1.5}$ and (c, d) $ZnO/In_{0.83}Ga_{0.17}O_{1.5}$ channel layers under (a, c) PBS and (b, d) NBS conditions. The stress conditions are as follows: PBS ($V_{GS} = V_{TH} + 20$ V) and NBS ($V_{GS} = V_{TH} - 20$ V).

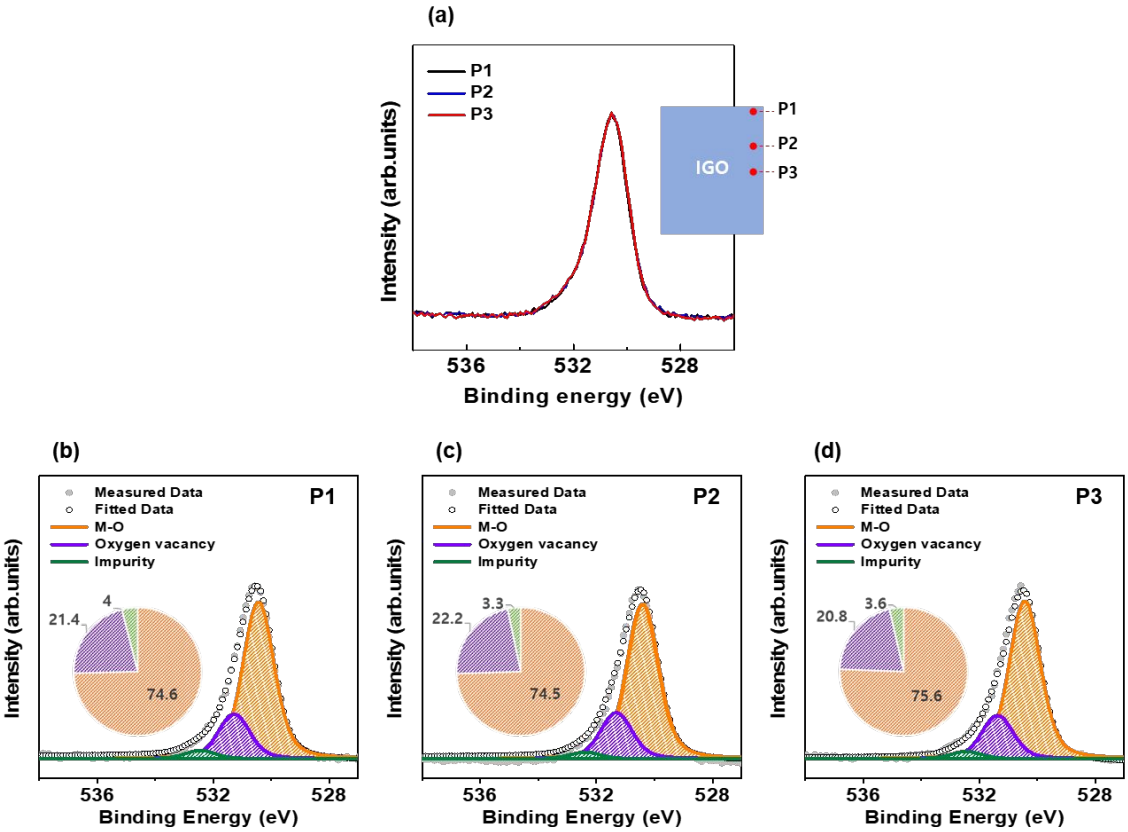

Figure S11. (a) O 1s XPS spectra of the $In_{0.83}Ga_{0.17}O_{1.5}$ sample recorded at each depth position (from the surface P1 to the bulk region P3). O 1s XPS spectra at different depth positions of (b) P1, (c) P2, and (d) P3, which were de-convoluted into three different sub-peaks consisting of lattice oxygen bonded with fully coordinated metal ions, oxygen deficient regions, and impurity-related species.

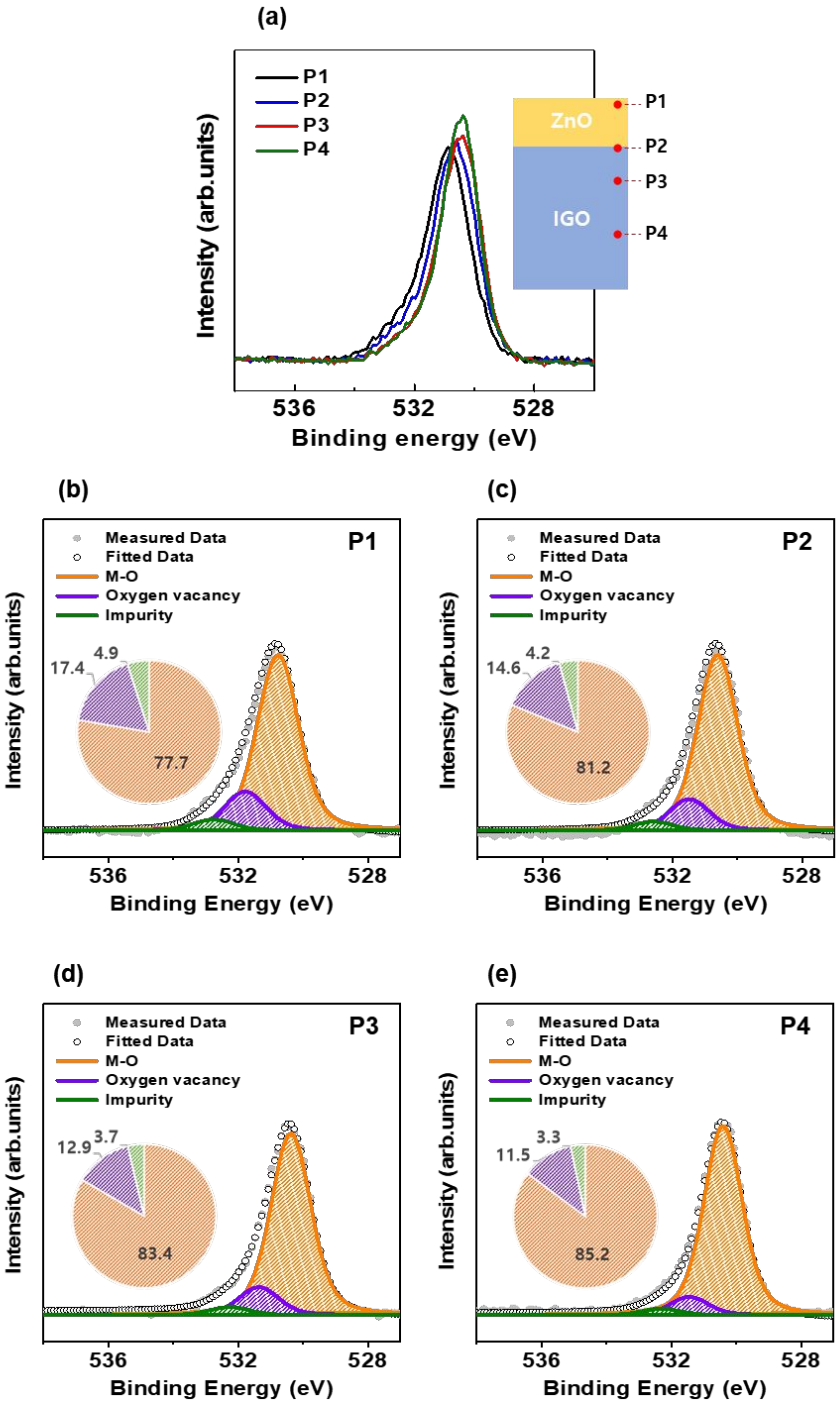

Figure S12. (a) O 1s XPS spectra of the ZnO/$In_{0.83}Ga_{0.17}O_{1.5}$ sample recorded at each depth position (from the surface P1 to the bulk region P4). O 1s XPS spectra at different depth positions of (b) P1, (c) P2, (d) P3, and (e) P4, which were de-convoluted into three different sub-peaks consisting of lattice

oxygen bonded with fully coordinated metal ions, oxygen deficient regions, and impurity-related species.

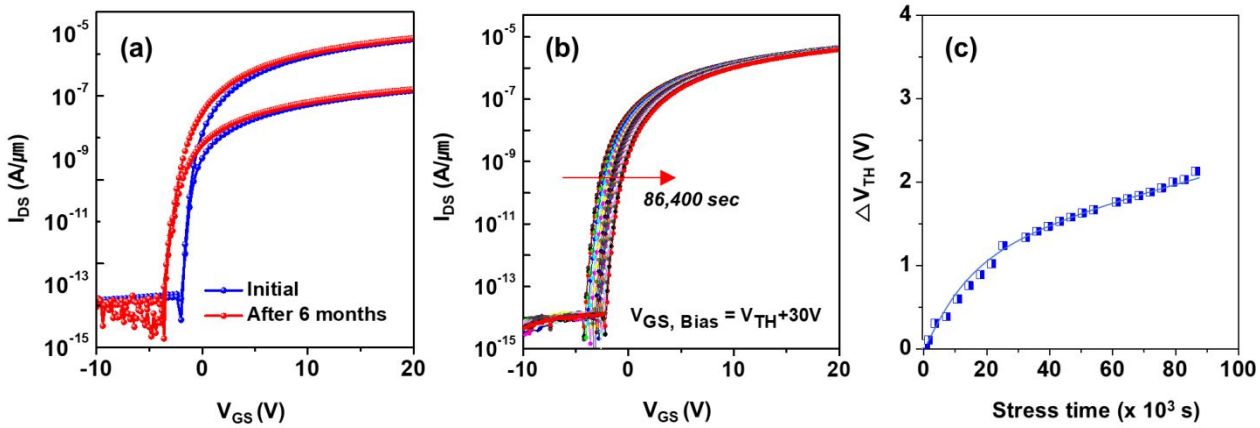

Figure S13. (a) Variations in transfer characteristics of the FETs with $ZnO/In_{0.83}Ga_{0.17}O_{1.5}$ heterojunction channel layer in an ambient environment for 6-months. (b) Variations in the transfer characteristics for the FET with $ZnO/In_{0.83}Ga_{0.17}O_{1.5}$ heterojunction channel layer under the gate bias of V_{TH} + 30 V for 24 hours (86,400 sec). (c) Corresponding V_{TH} shift as a function of PBS stress time.

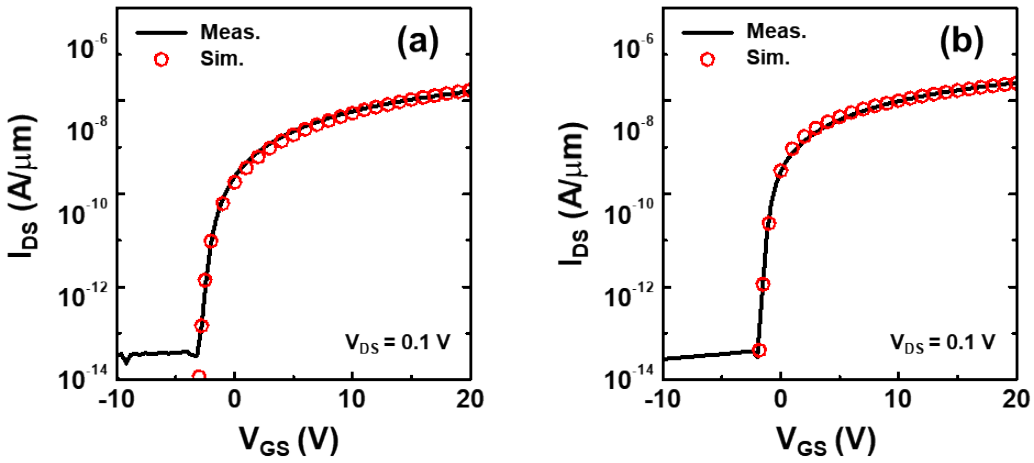

Figure S14. Measured and simulated transfer characteristics for FETs with the (a) $In_{0.83}Ga_{0.17}O_{1.5}$ single channel and (b) $ZnO/In_{0.83}Ga_{0.17}O_{1.5}$ heterojunction channel.

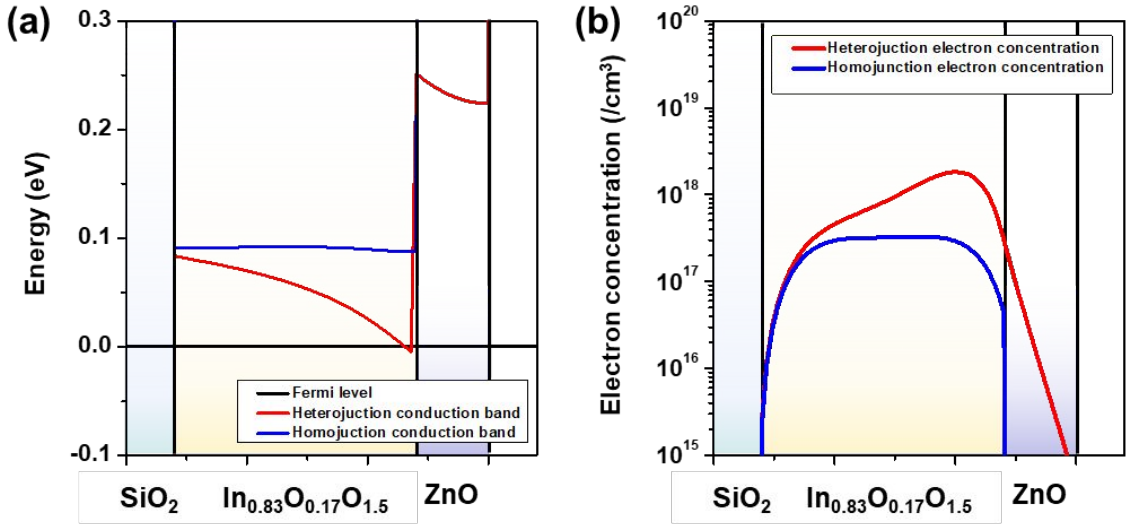

Figure S15. Simulated (a) energy band diagrams and (b) electron concentrations along the vertical direction from the gate dielectric/channel interface toward the back channel surface for FETs with the $In_{0.83}Ga_{0.17}O_{1.5}$ single channel and ZnO/$In_{0.83}Ga_{0.17}O_{1.5}$ heterojunction channel at flat-band conditions.

Table S1. Material parameters used in TCAD.

Parameter Symbol	Definition	Value
μ_{IGO} ($cm^2V^{-1}s^{-1}$)	Electron mobility in the conduction band of IGO	66
$N_{e.IGO}$ (cm^{-3})	Doping concentration of IGO	1.05×10^{17}
T_{IGO} (nm)	Thickness of IGO	10
m^*_{IGO}	Electron effective mass of IGO	$0.34m_0$
$E_{g.IGO}$ (eV)	Band gap energy of IGO	3.68
χ_{IGO} (eV)	Electron affinity of IGO	3.56
μ_{ZnO} ($cm^2V^{-1}s^{-1}$)	Electron mobility in the conduction band of ZnO	28
$N_{e.ZnO}$ (cm^{-3})	Doping concentration of ZnO	4×10^{18}
T_{ZnO} (nm)	Thickness of ZnO	3
m^*_{ZnO}	Electron effective mass of ZnO	$0.29m_0$
$E_{g.ZnO}$ (eV)	Band gap energy of ZnO	3.98
χ_{ZnO} (eV)	Electron affinity of ZnO	3.30

Table S2. Electrical parameters of the subgap density of states used in TCAD. The density of states for each subgap was modeled to have two exponential functions of acceptor-like states (i.e., g_{TA} and g_{DA}) and one Gaussian function of donor-like states (g_{OV}), respectively. The formulas are as follows:

$$g_{total}(E) = g_{TA}(E) + g_{DA}(E) + g_{OV}(E)$$
$$= N_{TA}exp\left(-\frac{Ec-E}{kT_{TA}}\right) + N_{DA}exp\left(-\frac{Ec-E}{kT_{DA}}\right) + N_{OV}exp\left(-\left(\frac{EOV-E}{kT_{OV}}\right)^2\right).$$

Parameter Symbol	Definition	Value
$N_{\text{TA.homo.}}$ ($\text{cm}^{-3}\text{eV}^{-1}$)	Density of the acceptor-like tail state of the IGO FET	1.7×10^{20}
$kT_{\text{TA.homo.}}$(eV)	Characteristic energy of the acceptor-like tail state of the IGO FET	0.011
$N_{\text{DA.homo.}}$ ($\text{cm}^{-3}\text{eV}^{-1}$)	Density of the acceptor-like deep state of the IGO FET	8.0×10^{18}
$kT_{\text{DA.homo.}}$ (eV)	Characteristic energy of the acceptor-like deep state of the IGO FET	0.12
$N_{\text{OV.homo.}}$ ($\text{cm}^{-3}\text{eV}^{-1}$)	Density of the shallow oxygen vacancy state of the IGO FET	1.2×10^{19}
$kT_{\text{OV.homo.}}$(eV)	Characteristic energy of the shallow oxygen vacancy state of the IGO FET	0.1
$E_{\text{OV.homo.}}$ (eV)	Mean energy of the shallow oxygen vacancy state of the IGO FET from Ec	0.05
$N_{\text{TA.hetero.}}$ ($\text{cm}^{-3}\text{eV}^{-1}$)	Density of the acceptor-like tail state of the ZnO/IGO FET	1.0×10^{20}
$kT_{\text{TA. hetero.}}$(eV)	Characteristic energy of the acceptor-like tail state of the ZnO/IGO FET	0.011
$N_{\text{DA. hetero.}}$ ($\text{cm}^{-3}\text{eV}^{-1}$)	Density of the acceptor-like deep state of the ZnO/IGO FET	7.0×10^{18}
$kT_{\text{DA. hetero.}}$(eV)	Characteristic energy of the acceptor-like deep state of the ZnO/IGO FET	0.12
$N_{\text{OV. hetero.}}$ ($\text{cm}^{-3}\text{eV}^{-1}$)	Density of the shallow oxygen vacancy state of the ZnO/IGO FET	7.3×10^{17}

$kT_{\text{OV. hetero.}}$(eV)	Characteristic energy of the shallow oxygen vacancy state of the ZnO/IGO FET	0.10
$E_{\text{OV. hetero.}}$(eV)	Mean energy of the shallow oxygen vacancy state of the ZnO/IGO FET from Ec	0.05